J. Fluid Mech. (1995), *vol.* 282, *pp.* 187–201

Inviscid instability of streamwise corner flow

By S. BALACHANDAR[1] AND M. R. MALIK[2]

[1] Department of Theoretical and Applied Mechanics, University of Illinois, Urbana, IL 61801, USA

[2] High Technology Corporation, 28 Research Drive, PO Box 7262, Hampton, VA 23666, USA

(Received 13 July 1993 and in revised form 29 July 1994)

Linear stability of the incompressible flow along a streamwise corner is studied by solving the two-dimensional eigenvalue problem governed by partial differential equations. It is found that this fully three-dimensional flow is subject to inviscid instability due to the inflectional nature of the streamwise velocity profile. The higher growth rates for the inviscid instability mode, which is symmetric about the corner bisector, as compared to the viscous Tollmien–Schlichting instability operative away from the corner, is consistent with the experimental findings that the corner flow transitions to turbulence earlier than the two-dimensional Blasius flow away from the corner.

1. Introduction

The last three decades have seen significant progress towards better understanding of the stability of flow over two-dimensional and swept wings. These advancements have greatly improved our prediction and control capabilities of the laminar–turbulent transition process. For further progress it is important to enhance our understanding of the effects of geometric complications such as wing–body junction, finite wing span, and surface roughness elements, which play an important role in the overall transition process. Here we consider the laminar stability of the flow along a streamwise corner, which can be considered as a model for the flow near a wing–body junction. The instability mechanisms induced by the streamwise corner will also help in assessing the effect of sidewalls on transitional and turbulent wind tunnel experiments. Understanding of the instability will also help us devise techniques for controlling transition in the corner flow.

The viscous flow along a corner that is formed by the intersection of two semi-infinite perpendicular plates (figure 1) is three-dimensional close to the corner due to the strong interaction of the boundary layers on the two perpendicular walls. The basic laminar flow permits a similarity solution under the boundary layer assumption. The governing self-similar boundary layer equations appropriate for the corner region, which blends with the two-dimensional Blasius boundary layer and the outer potential flow away from the cornerline, were obtained by Rubin (1966). Numerical solutions to these governing equations (Rubin & Grossman 1971; Ghia 1975) exhibit a secondary cross-stream flow which is directed towards the corner along the two walls and directed away from the corner along the corner bisector. The resulting streamwise velocity profile along the corner bisector is inflectional in nature. Therefore the three-dimensional boundary layer near a streamwise corner is susceptible to inviscid instability, while the two-dimensional Blasius counterpart is only subjected to milder viscous instability.

Experiments on corner layers by Barclay (1973), El-Gamal & Barclay (1978) and

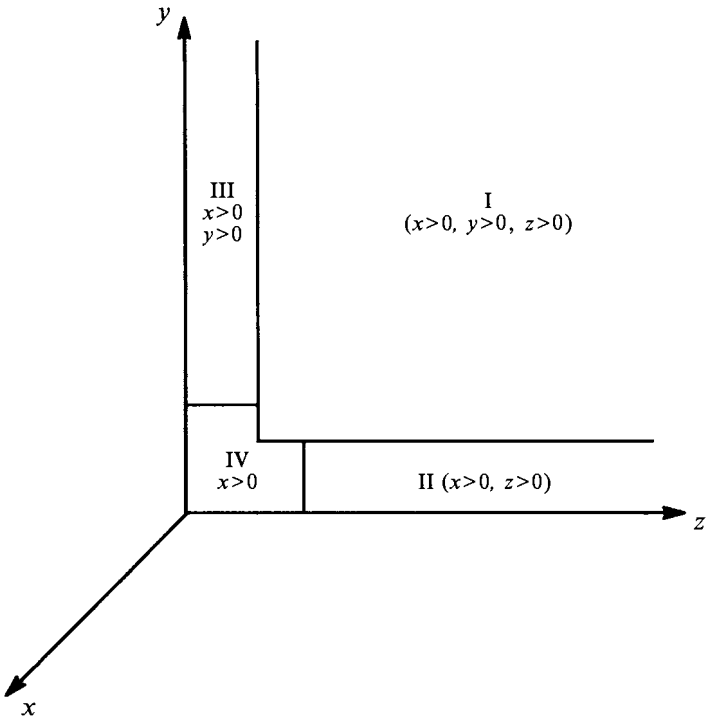

FIGURE 1. Streamwise corner flow geometry and the coordinate system used.

Zamir & Young (1970, 1979) have yielded contrasting results for the laminar self-similar velocity profile. The differences among these experimental results highlight the exceptional sensitivity of the laminar corner layer solution to differences in the shape of the leading edge and streamwise pressure gradients (see Zamir 1981). This sensitivity to measurements can be attributed to the early instability of the corner layer compared to the Blasius boundary layer. Based on his favourable pressure gradient experiments, Zamir (1981) observes that the zero-pressure-gradient corner layer becomes transitional at a Reynolds number of around 10^4, while the critical Reynolds number for a zero-pressure-gradient flat-plate boundary layer is an order of magnitude higher, around 10^5.

Lakin & Hussaini (1984) considered the stability of the corner flow sufficiently away from the cornerline in the blending region, where the streamwise and wall normal velocities are given by the Blasius solution with a superimposed secondary spanwise velocity induced by the corner. Solutions to the stability equations were obtained with a critical layer analysis. Recently, Dhanak (1993) studied the stability of the blending boundary layer numerically, employing the same governing equations as those of Lakin & Hussaini but emphasized the importance of enforcing appropriate symmetry boundary conditions along the corner bisector, instead of the usual asymptotic boundary conditions at infinity for the one-dimensional problem. Sufficiently far away from the cornerline stability results for the Blausius profile were obtained and as the cornerline is approached the blending layer was observed to become increasingly unstable. The one-dimensional stability analysis ignores any spanwise variation of the mean flow, whereas the actual flow is three-dimensional and the approach towards the Blasius boundary layer is only algebraic (Pal & Rubin 1971). The blending layer stability results display the correct qualitative trend which agrees with experimental

results but the quantitative predictions need to be verified with a two-dimensional stability analysis.

Here we will retain the strong dependence of the corner boundary layer along the two wall normal directions and consider the stability of this flow with a locally parallel assumption along the streamwise direction. The resulting two-dimensional stability analysis results in an eigenvalue problems which poses far greater computational challenges than the one-dimensional counterpart. To simplify the analysis and computations, we will restrict attention to an inviscid analysis through an extended Rayleigh equation (a partial differential equation). The inviscid analysis should be adequate to capture the qualitative features of the dominant instability mechanism arising from the inflectional nature of the streamwise velocity component.

Instability of inviscid modes in a boundary layer does not guarantee that they remain unstable in the corresponding viscous problem. But there are a number of examples in fluid mechanics where inviscid modes are also found to be unstable at finite Reynolds numbers. For example, Stuart (see Gregory, Stuart & Walker 1955) considered the three-dimensional boundary layer on a rotating disk and found crossflow instability using an inviscid analysis. Much later Malik, Wilkinson & Orszag (1981) performed a corresponding viscous analysis and found the boundary layer to be unstable to crossflow disturbances provided the Reynolds number is above a finite critical value. In fact, this inviscid instability is the main cause of transition in a swept-wing boundary layer. Similarly, the second-mode disturbance in a hypersonic boundary layer (Mack 1984) is inviscid in nature but is also captured in viscous analysis. The second-mode instability is found to be responsible for hypersonic boundary layer transition at finite Reynolds numbers (Stetson *et al.* 1983).

2. Mathematical formulation: mean flow

The viscous flow along the corner that is formed by the intersection of two semi-infinite perpendicular flat plates (figure 1) can be simplified with the boundary layer theory. Unlike flat plate and infinite wing geometries, the corner flow is three-dimensional (all three velocity components exist and they are functions of all three coordinates). Sufficiently far way from both the flat plates (region I) the flow can be modelled as potential flow. Close to the plates but far away from the corner line (regions II and III) the mean flow is nearly two-dimensional and depends only on the x- and y-coordinates in region II and on the x- and z-coordinates in region III. These two-dimensional blending boundary layers are primarily Blasius boundary layers, but with a superposed transverse flow. In the region close to the cornerline (region IV) the coupling that is created by the mutual interaction results in a strongly three-dimensional boundary layer. The flow in this corner region, termed the 'corner layer' is the subject matter of this paper.

The governing three-dimensional boundary layer equations appropriate within the corner layer can be written in a self-similar form as follows (Rubin 1966):

$$-\tilde{\eta}\frac{\partial \hat{u}}{\partial \tilde{\eta}}-\tilde{\zeta}\frac{\partial \hat{u}}{\partial \tilde{\zeta}}+\frac{\partial \hat{v}}{\partial \tilde{\eta}}+\frac{\partial \hat{w}}{\partial \tilde{\zeta}}=0, \tag{1a}$$

$$-\tilde{\eta}\hat{u}\frac{\partial \hat{u}}{\partial \tilde{\eta}}-\tilde{\zeta}\hat{u}\frac{\partial \hat{u}}{\partial \tilde{\zeta}}+\hat{v}\frac{\partial \hat{u}}{\partial \tilde{\eta}}+\hat{w}\frac{\partial \hat{u}}{\partial \tilde{\zeta}}=\frac{\partial^2 \hat{u}}{\partial \tilde{\eta}^2}+\frac{\partial^2 \hat{u}}{\partial \tilde{\zeta}^2}, \tag{1b}$$

$$-\hat{u}\hat{v}-\tilde{\eta}\hat{u}\frac{\partial \hat{v}}{\partial \tilde{\eta}}-\tilde{\zeta}\hat{u}\frac{\partial \hat{v}}{\partial \tilde{\zeta}}+\hat{v}\frac{\partial \hat{v}}{\partial \tilde{\eta}}+\hat{w}\frac{\partial \hat{v}}{\partial \tilde{\zeta}}=-\frac{\partial \hat{p}}{\partial \tilde{\eta}}+\frac{\partial^2 \hat{v}}{\partial \tilde{\eta}^2}+\frac{\partial^2 \hat{v}}{\partial \tilde{\zeta}^2}, \tag{1c}$$

$$-\hat{u}\hat{w}-\tilde{\eta}\hat{u}\frac{\partial\hat{w}}{\partial\tilde{\eta}}-\tilde{\xi}\hat{u}\frac{\partial\hat{w}}{\partial\tilde{\xi}}+\hat{v}\frac{\partial\hat{w}}{\partial\tilde{\eta}}+\hat{w}\frac{\partial\hat{w}}{\partial\tilde{\xi}}=-\frac{\partial\hat{p}}{\partial\tilde{\xi}}+\frac{\partial^2\hat{w}}{\partial\tilde{\eta}^2}+\frac{\partial^2\hat{w}}{\partial\tilde{\xi}^2}, \tag{1d}$$

where $\tilde{\eta}$ and $\tilde{\xi}$ are the non-dimensional boundary layer coordinates along the wall normal directions y and z given by

$$\tilde{\eta}=\frac{y}{(2xx^*)^{1/2}}Re^{1/2} \quad \text{and} \quad \tilde{\xi}=\frac{z}{(2xx^*)^{1/2}}Re^{1/2}, \tag{2}$$

where the Reynolds number is defined as $Re = Ux^*/\nu$. The dependent variables $\hat{u}$, $\hat{v}$, $\hat{w}$ and $\hat{p}$ are the non-dimensional velocity components and pressure and are related to their dimensional values u, v and w and p through the following relations:

$$\hat{u}=\frac{u}{U}, \quad \hat{v}=\frac{\sqrt{2}v}{U}\left(\frac{x}{x^*}\right)^{1/2}Re^{1/2}, \quad \hat{w}=\frac{\sqrt{2}w}{U}\left(\frac{x}{x^*}\right)^{1/2}Re^{1/2}, \quad \hat{p}=\frac{2p}{\rho U^2}\left(\frac{x}{x^*}\right)Re. \tag{3}$$

Here U is the free stream velocity, x^* is the dimensional distance from the leading edge, ρ and ν are the density and kinematic viscosity of the fluid. The above self-similar form of the corner layer avoids explicit dependence of the corner layer equations (1) on the streamwise direction, x. Equation (1) is only the first of an infinite set of equations that can be obtained for the asymptotic solution of the corner layer and is exact in the limit of $Re\to\infty$.

The elliptic nature of the governing equation (1) requires boundary conditions for $\hat{u},\hat{v},\hat{w}$ on the four bounding lines $\tilde{\eta}=0$, $\tilde{\xi}=0$, $\tilde{\eta}=\tilde{\eta}_{max}\to\infty$, $\tilde{\xi}=\tilde{\xi}_{max}\to\infty$. The proper boundary conditions on the two walls are no-slip and no-penetration. The asymptotic boundary conditions appropriate in the limit of $\tilde{\xi}_{max}\to\infty$, and $\tilde{\eta}<\tilde{\xi}$, should blend with the blending boundary layer (region II). By symmetry the same boundary condition applies in the limit of $\tilde{\eta}_{max}\to\infty$. These asymptotic boundary conditions can be expressed as the following expansion in inverse powers of distance from the cornerline (Pal & Rubin 1971):

$$\hat{u}(\tilde{\eta},\tilde{\xi}_{max})=\hat{u}_0(\tilde{\eta})+\frac{\hat{u}_1(\tilde{\eta})}{\tilde{\xi}_{max}}+\frac{\hat{u}_2(\tilde{\eta})}{\tilde{\xi}^2_{max}}+\frac{\hat{u}_3(\tilde{\eta})}{\tilde{\xi}^3_{max}}+O(\tilde{\xi}^{-4}), \tag{4a}$$

$$\hat{v}(\tilde{\eta},\tilde{\xi}_{max})=\hat{v}_0(\tilde{\eta})+\frac{\hat{v}_1(\tilde{\eta})}{\tilde{\xi}_{max}}+\frac{\hat{v}_2(\tilde{\eta})}{\tilde{\xi}^2_{max}}+\frac{\hat{v}_3(\tilde{\eta})}{\tilde{\xi}^3_{max}}+O(\tilde{\xi}^{-4}), \tag{4b}$$

$$\hat{w}(\tilde{\eta},\tilde{\xi}_{max})=\hat{w}_1(\tilde{\eta})+\frac{\hat{w}_2(\tilde{\eta})}{\tilde{\xi}_{max}}+\frac{\hat{w}_3(\tilde{\eta})}{\tilde{\xi}^2_{max}}+O(\tilde{\xi}^{-3}), \tag{4c}$$

$$\hat{p}(\tilde{\eta},\tilde{\xi}_{max})=\hat{p}_0(\tilde{\eta})+\frac{\hat{p}_1(\tilde{\eta})}{\tilde{\xi}_{max}}+\frac{\hat{p}_2(\tilde{\eta})}{\tilde{\xi}^2_{max}}+\frac{\hat{p}_3(\tilde{\eta})}{\tilde{\xi}^3_{max}}+O(\tilde{\xi}^{-4}). \tag{4d}$$

The zeroth-order boundary conditions, $\hat{u}_0$, $\hat{v}_0$ and $\hat{p}_0$, are nothing but the Blasius boundary layer solutions. The first-order streamwise and wall normal velocities can be shown to be zero (Pal & Rubin 1971) and the only first-order effect of the corner is to induce the secondary flow, $\hat{w}_1$, towards the corner along the bottom wall. The higher-order terms in the above equation have been obtained by Pal & Rubin (1971) by requiring a simultaneous matching of the corner layer with the outer potential flow as $\tilde{\eta},\tilde{\xi}\to\infty$. Thus (4) provides an asymptotically accurate higher-order boundary condition which can be applied at the outer boundaries of a computational domain that has been truncated to a large but finite $\tilde{\eta}=\tilde{\eta}_{max}$ and $\tilde{\xi}=\tilde{\xi}_{max}$. The above equation displays the algebraic decay towards the Blasius boundary layer as $\tilde{\xi}\to\infty$.

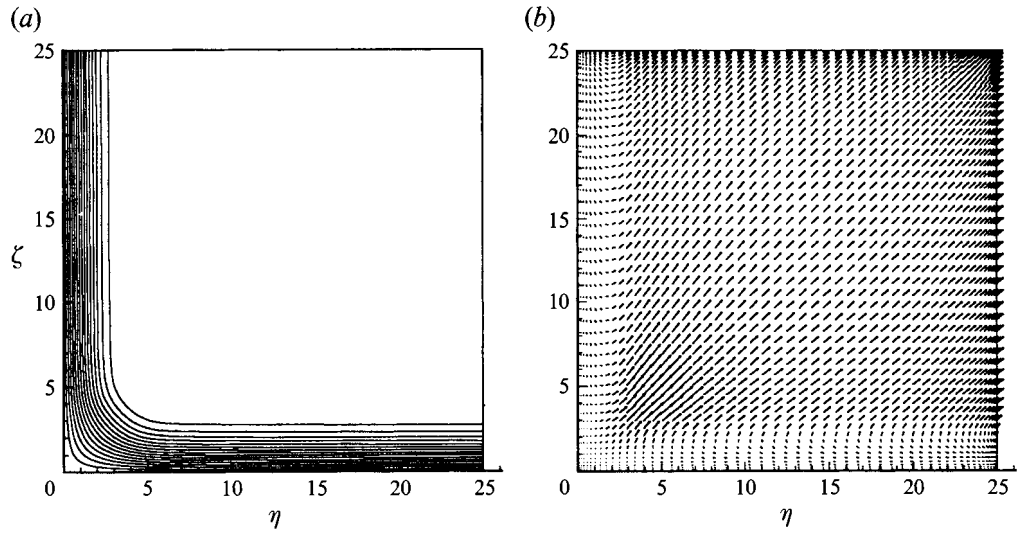

FIGURE 2. (*a*) Contour plot of the streamwise component of the mean velocity field. There are 19 contour lines running from 0.05 near the walls to 0.95 away from the walls. Also shown is a vector plot of the cross-stream velocity components, (*b*).

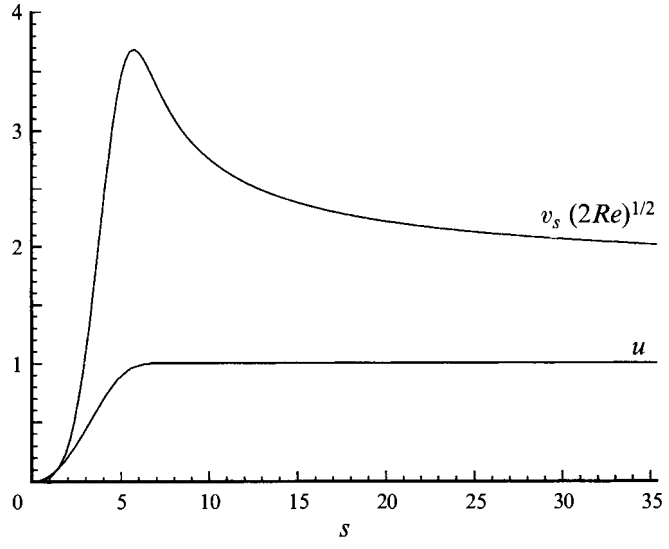

FIGURE 3. Velocity components along the streamwise direction and along the corner bisector plotted against distance from the cornerline along the corner bisector (*s*). Owing to boundary layer scaling the actual velocity component along the corner bisector is order $(Re)^{1/2}$ smaller than the streamwise component.

The governing equations (1) can be solved with wall boundary conditions and asymptotic outer boundary conditions (equation (4)) to obtain the laminar corner layer. This problem of obtaining the corner mean flow has been addressed by many authors (Carrier 1947; Pearson 1957; Rubin & Grossman 1971; Desai & Mangler 1974; Ghia 1975) with varying degrees of approximations applied to the governing equations and the boundary conditions. Here we have employed a Chebyshev-spectral ADI technique in order to solve the corner layer equations. The spectral discretization will provide the exponential accuracy needed for accurate stability calculations. In the

numerical solution the outer boundary is placed at $\tilde{\eta}_{max} = \tilde{\zeta}_{max} = 25$ and the computational domain is discretized with 85 Chebyshev Gauss–Lobatto points along both the $\tilde{\eta}$- and $\tilde{\zeta}$-directions. A third-order-accurate asymptotic boundary condition (equation (4)) is applied at the outer edges of the computational domain. Even-symmetry about the corner bisector is imposed on the mean flow solution in order to accelerate convergence towards the final solution. Results obtained from this technique compare favourably with those of Rubin & Grossman (1971) and Ghia (1975). Figure 2 shows contours of streamwise velocity and a vector plot of the cross-stream velocity. Figure 3 shows the velocity profiles plotted along the corner bisector. An inflection point in the streamwise velocity profile at $\tilde{\eta} = \tilde{\zeta} \approx 2.4$ is evident.

3. Stability analysis

The stability of the laminar base flow to small perturbations can be investigated through the standard linear stability analysis. A quasi-parallel flow assumption for the base flow along the streamwise direction will be made about the point $x = x^*$, by neglecting the slow streamwise variation of the mean flow. In the stability analysis the streamwise coordinate is centred about the point $x = x^*$ and the two wall normal coordinates are non-dimensionalized uniformly with $\sqrt{2x^* Re^{-1/2}}$ as the lengthscale defining a new set of non-dimensional coordinates as

$$\xi = \frac{x - x^*}{\sqrt{2x^*}} Re^{1/2}, \quad \eta = \frac{y}{\sqrt{2x^*}} Re^{1/2}, \quad \zeta = \frac{z}{\sqrt{2x^*}} Re^{1/2}. \tag{5}$$

Similarly all three components of velocity are uniformly non-dimensionalized by the free-stream velocity U, resulting in a non-dimensional locally parallel mean flow ($\hat{u}_m$, $\hat{v}_m$, $\hat{w}_m$) given by

$$\hat{u}_m = \hat{u}, \quad \hat{v}_m = \hat{v}(2Re)^{-1/2}, \quad \hat{w}_m = \hat{w}(2Re)^{-1/2}. \tag{6}$$

Velocity and pressure perturbations of the following form (normal mode anastaz) can be superimposed on to the mean flow,

$$u_p = \hat{u}_p(\eta, \zeta) \exp[\mathrm{i}(\alpha\xi - \omega t)], \quad v_p = \hat{v}_p(\eta, \zeta) \exp[\mathrm{i}(\alpha\xi - \omega t)], \tag{7a, b}$$

$$w_p = \hat{w}_p(\eta, \zeta) \exp[\mathrm{i}(\alpha\xi - \omega t)], \quad p_p = \hat{p}_p(\eta, \zeta) \exp[\mathrm{i}(\alpha\xi - \omega t)], \tag{7c, d}$$

and the total velocity and pressure when substituted into the Navier–Stokes equation and the incompressibility condition and linearized results in the following stability equations:

$$\hat{u}_m \mathrm{i}\alpha\hat{u}_p + \hat{v}_m \frac{\partial \hat{u}_p}{\partial \eta} + \hat{w}_m \frac{\partial \hat{u}_p}{\partial \zeta} + \hat{v}_p \frac{\partial \hat{u}_m}{\partial \eta} + \hat{w}_p \frac{\partial \hat{u}_m}{\partial \zeta} + \mathrm{i}\alpha\hat{p}_p - \mathrm{L}\hat{u}_p = \mathrm{i}\omega\hat{u}_p, \tag{8a}$$

$$\hat{u}_m \mathrm{i}\alpha\hat{v}_p + \hat{v}_m \frac{\partial \hat{v}_p}{\partial \eta} + \hat{w}_m \frac{\partial \hat{v}_p}{\partial \zeta} + \hat{v}_p \frac{\partial \hat{v}_m}{\partial \eta} + \hat{w}_p \frac{\partial \hat{v}_m}{\partial \zeta} + \frac{\partial \hat{p}_p}{\partial \eta} - \mathrm{L}\hat{v}_p = \mathrm{i}\omega\hat{v}_p, \tag{8b}$$

$$\hat{u}_m \mathrm{i}\alpha\hat{w}_p + \hat{v}_m \frac{\partial \hat{w}_p}{\partial \eta} + \hat{w}_m \frac{\partial \hat{w}_p}{\partial \zeta} + \hat{v}_p \frac{\partial \hat{w}_m}{\partial \eta} + \hat{w}_p \frac{\partial \hat{w}_m}{\partial \zeta} + \frac{\partial \hat{p}_p}{\partial \zeta} - \mathrm{L}\hat{w}_p = \mathrm{i}\omega\hat{w}_p, \tag{8c}$$

$$\mathrm{i}\alpha\hat{u}_p + \frac{\partial \hat{v}_p}{\partial \eta} + \frac{\partial \hat{w}_p}{\partial \zeta} = 0, \tag{8d}$$

where the operator

$$\mathrm{L} = \frac{1}{(2Re)^{1/2}} \left[-\alpha^2 + \frac{\partial^2}{\partial \eta^2} + \frac{\partial^2}{\partial \zeta^2} \right].$$

In the above temporal stability formulation, the input parameters to the stability analysis, α and Re, are respectively the streamwise wavenumber and Reynolds number

and ω is the resulting complex eigenvalue whose real part ω_r represents the disturbance frequency and imaginary part ω_i corresponds to the disturbance growth rate. Hence if $\omega_i > 0$, corner flow is susceptible to unstable small amplitude disturbances.

Boundary conditions for the two-dimensional viscous stability analysis are no-slip and no-penetration conditions at the solid boundaries. Appropriate outer velocity boundary conditions for the stability analysis depend on the disturbance mode to be captured. Inflectional instability modes can be represented both by homogeneous Dirichlet and homogeneous Neumann boundary conditions. Viscous modes which become two-dimensional Tollmein–Schlichting modes in the limit of $\eta = \zeta \to \infty$ can be captured with homogeneous Neumann outer boundary condition. Viscous modes which asymptotically merge with oblique Tollmein–Schlichting modes in the limit of $\eta = \zeta \to \infty$ require homogeneous mixed boundary condition. In all the above cases, artificial pressure boundary conditions can be avoided with a fully staggered grid.

Upon spatial discretization, the above stability equations (8) along with the boundary conditions reduce to a generalized matrix eigenvalue problem. With N grid points along each of the η- and ζ-directions the size of the matrix eigenvalue problem is nearly $4N^2 \times 4N^2$ and the computational cost of solving the eigenvalue problem using standard eigenvalue routines (from IMSL and EISPACK) scales as $O(N^6)$. Therefore computational time and memory places stringent limitations on the spatial resolution. The following symmetry conditions about the corner bisector:

symmetric mode:

$$\hat{u}_p(\eta, \zeta) = \hat{u}_p(\zeta, \eta), \quad \hat{v}_p(\eta, \zeta) = \hat{w}_p(\zeta, \eta), \quad \hat{p}_p(\eta, \zeta) = \hat{p}_p(\zeta, \eta); \tag{9a}$$

antisymmetric mode:

$$\hat{u}_p(\eta, \zeta) = -\hat{u}_p(\zeta, \eta), \quad \hat{v}_p(\eta, \zeta) = -\hat{w}_p(\zeta, \eta), \quad \hat{p}_p(\eta, \zeta) = -\hat{p}_p(\zeta, \eta), \tag{9b}$$

can be used to reduce the size of the matrix four-fold, but the eigenvalue problem still remains formidable. Therefore, here we consider two simpler problems: (i) one-dimensional bisector stability analysis, where the stability of the bisector profile alone is considered; (ii) two-dimensional inviscid stability analysis in the limit of $Re \to \infty$. The inviscid approximation reduces the size of the discretized matrix sixteen-fold and the computational cost sixty-four-fold over the corresponding viscous stability analysis.

3.1. *Bisector instability*

We will first consider the effect of the inflectional profile by studying the simpler problem of the one-dimensional stability of the velocity profile along the corner bisector. Instead of the Cartesian coordinates η and ζ a new orthogonal coordinate system s and r will be considered, where s is along the corner bisector. In the transformed coordinates a locally parallel flow assumption is made by ignoring the variations in the mean flow along the streamwise ξ- and tangential r-directions and the stability of this one-dimensional base flow to disturbances of the following form is considered:

$$\begin{Bmatrix} \hat{u}_p(s) \\ \hat{v}_p(s) \\ \hat{w}_p(s) \\ \hat{p}_p(s) \end{Bmatrix} \exp\left[\mathrm{i}(\alpha\xi + \beta r - \omega t)\right]. \tag{10}$$

The results obtained from this bisector stability analysis will be presented below to provide qualitative understanding of the effect of the inflectional nature of the base flow on the overall stability. Figure 4 shows the temporal growth rate (imaginary part

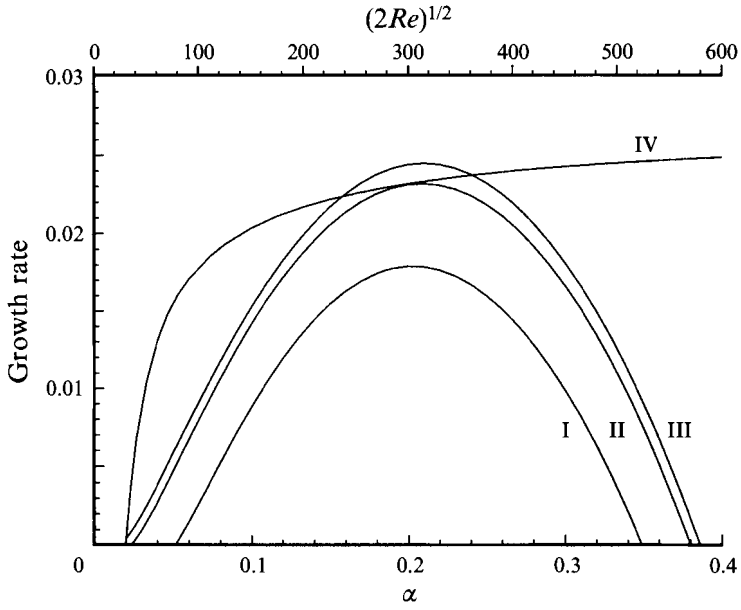

FIGURE 4. Growth rate obtained from the bisector instability analysis *vs.* α: case I, $Re = 5000$; case II, $Re = 4.5 \times 10^4$; case III, $Re = 1.25 \times 10^5$. Case IV: growth rate *vs.* Re for $\alpha = 0.21$.

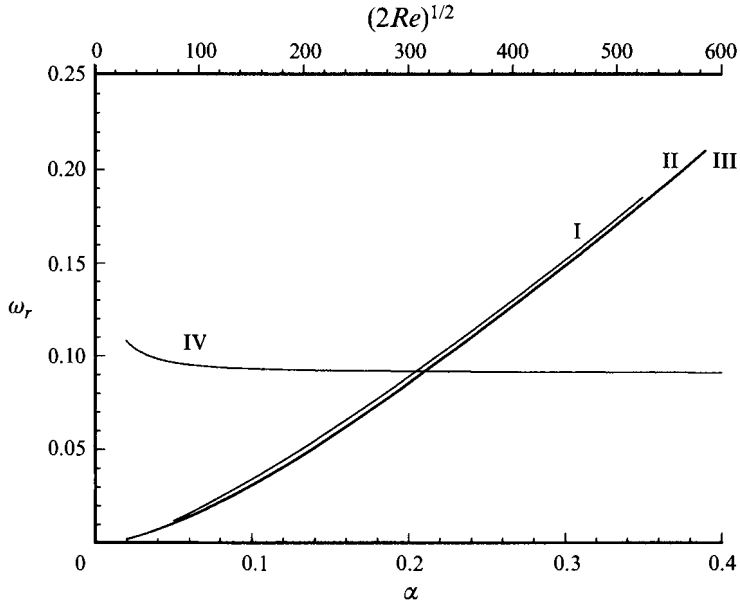

FIGURE 5. Frequency obtained from the bisector instability analysis *vs.* α: case I, $Re = 5000$; case II, $Re = 4.5 \times 10^4$; case III, $Re = 1.25 \times 10^5$. Case IV: frequency *vs.* Re for $\alpha = 0.21$.

of ω) of the disturbance plotted against streamwise wavenumber α at three different Reynolds numbers, $Re = 5000$ (case I); 4.5×10^4 (case II) and 1.25×10^5 (case III). Two-dimensional disturbances corresponding to $\beta = 0$ are the most amplified and results corresponding to this case only will be presented. The outer edge of the computational domain is chosen to be $s_{max} = 25$ and is discretized by 85 Chebyshev Gauss–Lobatto points; asymptotic boundary conditions are applied at the outer edge.

The results presented are well converged and show insensitivity to the exact number of grid points, location and nature of the outer boundary condition. Also plotted in figure 4 is growth rate *vs.* $(Re)^{1/2}$ for $\alpha = 0.21$ (case IV). A critical Reynolds number of $Re_{crit} = 435.0$ is obtained and the corresponding critical streamwise wavelength, $\alpha_{crit} = 0.21$ and the critical frequency, $(\omega_{crit})_r = 0.1$. This result, compared with the critical Reynolds number of 9.1×10^4 for the Blasius profile, shows that the inflection point induced by the streamwise corner has the potential to decrease the critical Reynolds number by as much as two orders of magnitude. Owing to its inviscid nature, the growth rates for the bisector profile are also much larger than those of the Tollmien–Schlichting disturbance in the Blasius boundary layer. Figure 5 shows the frequency (ω_r) variation corresponding to the four cases discussed above. As expected the frequency varies linearly with α for large values of the wavenumber and is almost independent of the Reynolds number.

3.2. *The two-dimensional inviscid eigenvalue problem*

With the above encouraging results we will consider the two-dimensional inviscid instability of the corner flow in the limit of $Re \to \infty$. In this limit the viscous terms drops out of (8). It should also be noted that in the limit of infinite Reynolds number the mean flow is purely streamwise, since in the boundary layer approximation the cross-stream velocities, $\hat{v}_m$ and $\hat{w}_m$, are $O(Re^{-1/2})$ smaller than the streamwise velocity. Even in this limit, the secondary effect of the cross-stream velocities and the associated streamwise vorticity is still present in terms of the inflectional nature of the streamwise velocity field. Equation (8) can therefore be simplified to

$$-\mathrm{i}\omega\hat{u}_p + \hat{u}_m\,\mathrm{i}\alpha\hat{u}_p + \hat{v}_p\frac{\partial\hat{u}_m}{\partial\eta} + \hat{w}_p\frac{\partial\hat{u}_m}{\partial\zeta} = -\mathrm{i}\alpha\hat{p}_p, \tag{11a}$$

$$-\mathrm{i}\omega\hat{v}_p + \hat{u}_m\,\mathrm{i}\alpha\hat{v}_p = -\frac{\partial\hat{p}_p}{\partial\eta}, \tag{11b}$$

$$-\mathrm{i}\omega\hat{w}_p + \hat{u}_m\,\mathrm{i}\alpha\hat{w}_p = -\frac{\partial\hat{p}_p}{\partial\zeta}, \tag{11c}$$

$$\mathrm{i}\alpha\hat{u}_p + \frac{\partial\hat{v}_p}{\partial\eta} + \frac{\partial\hat{w}_p}{\partial\zeta} = 0. \tag{11d}$$

The above linear momentum and continuity equations can be combined to form the following single higher-order equation for the pressure perturbation (Hall & Horseman 1990):

$$-\alpha^2\hat{u}_m\hat{p}_p + \hat{u}_m\frac{\partial^2\hat{p}_p}{\partial\eta^2} - 2\frac{\partial\hat{u}_m}{\partial\eta}\frac{\partial\hat{p}_p}{\partial\eta} + \hat{u}_m\frac{\partial^2\hat{p}_p}{\partial\zeta^2} - 2\frac{\partial\hat{u}_m}{\partial\zeta}\frac{\partial\hat{p}_p}{\partial\zeta} = \frac{\omega}{\alpha}\mathrm{L}\hat{p}_p. \tag{12}$$

We will employ a spectral methodology (Canuto *et al.* 1988) for solving the above eigenvalue problem with Chebyshev discretization along the η- and ζ-directions. With this spatial discretization (12) reduces to a generalized matrix eigenvalue problem of the form

$$\boldsymbol{A}\hat{\boldsymbol{p}}_p = \frac{\omega}{\alpha}\boldsymbol{B}\hat{\boldsymbol{p}}_p. \tag{13}$$

With N grid points along each of the η- and ζ-directions the size of the matrix eigenvalue problem is $N^2 \times N^2$. Symmetry conditions about the corner bisector are used to reduce the size of the matrix four-fold.

In the inviscid limit the appropriate boundary condition to be applied on the solid boundaries for the velocity eigenfunctions is no penetration. From (11*b*) and (11*c*) the

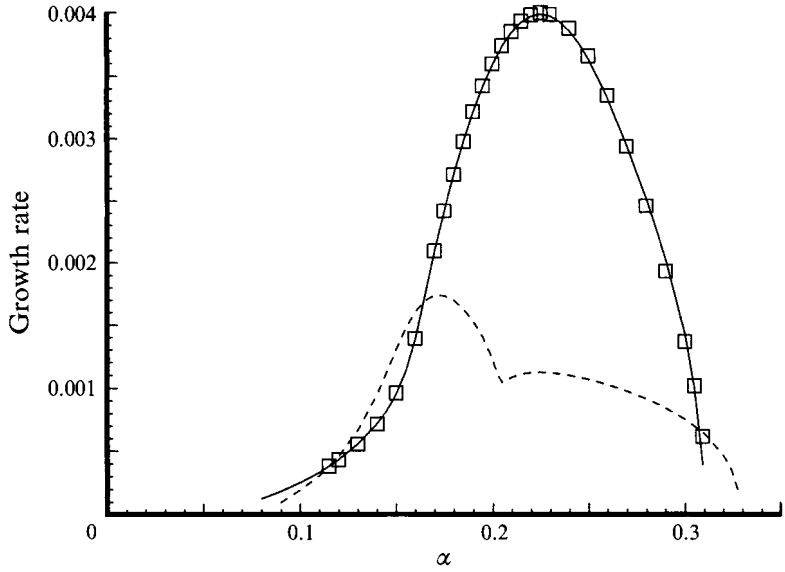

FIGURE 6. Growth rate *vs.* α obtained from the inviscid instability analysis for the first two most unstable disturbance modes. Solid line corresponds to the most unstable mode and the dashed line corresponds to the second most unstable mode. The symbols correspond to the homogeneous Neumann pressure boundary condition and the lines to the homogeneous Dirichlet condition.

corresponding pressure boundary conditions on the solid boundaries are zero normal derivatives. The computational domain will be truncated to be a finite square and the outer boundary conditions will be imposed at $\eta = \eta_{max}$ and $\zeta = \zeta_{max}$. The appropriate boundary condition for pressure at these outer boundaries is not clear. But far away from the corner ($\eta = \eta_{max}, \zeta = \zeta_{max}$) the streamwise velocity profile is not inflectional and will not support inviscid instability. Therefore, it is reasonable to assume that $\hat{p}_p = 0$ at $\eta = \eta_{max}$ and $\zeta = \zeta_{max}$. In any case, the eigenvalue problem was solved with both Dirichlet ($\hat{p}_p = 0$) and Neumann ($\partial\hat{p}_p/\partial\eta = \partial\hat{p}_p/\partial\zeta = 0$) boundary conditions and the sensitivity of the stability results to the placement of the outer boundary at $\eta = \eta_{max}$ and $\zeta = \zeta_{max}$ and to the number of grid points was also considered. Based on these sensitivity tests $\eta_{max} = \zeta_{max} = 25$ with 55 Chebyshev Gauss–Lobatto points along both the η- and ζ-directions was found adequate to provide well converged results. Accurate mean flow at these grid points was obtained by a spectral interpolation scheme. Both Dirichlet and Neumann boundary conditions for pressure at the outer boundaries yielded identical results to five decimal places.

Only results for the symmetric disturbance case will be presented below. The antisymmetric disturbances did not provide any growing solution. This result is to be expected since the symmetric disturbances have their peak value along the corner bisector, where the base flow is inflectional. On the other hand, antisymmetric disturbances result in zero pressure and streamwise velocity perturbations along the corner bisector. Although, there are no growing antisymmetric modes in the inviscid limit, we anticipate growing antisymmetric (Tollmien–Schlichting-like) viscous modes in a full viscous stability problem, but their growth rate will still be smaller than the corresponding symmetric mode.

In figure 6 the growth rate of the most unstable inviscid instability mode is plotted as a function of the streamwise wavenumber. The continuous curve corresponds to the case where the homogeneous Dirichlet condition is used at the outer boundaries for the

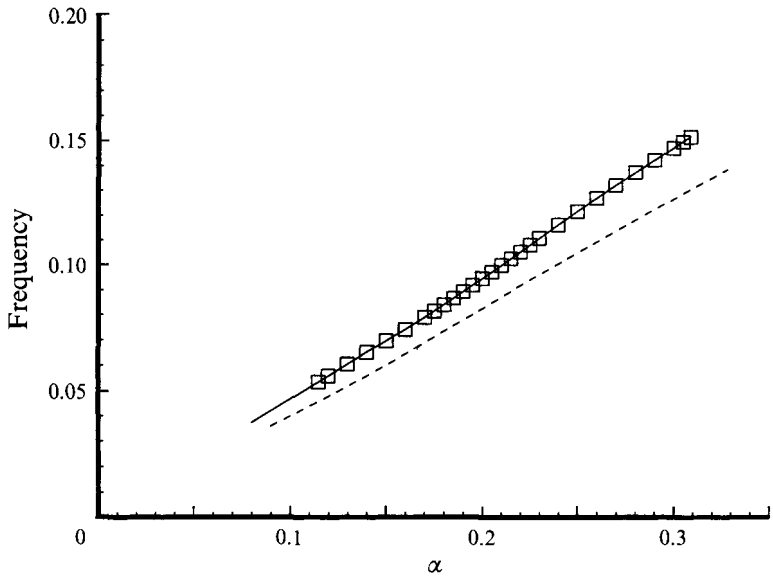

FIGURE 7. Frequency *vs.* α obtained from the inviscid instability analysis for the first two most unstable disturbance modes. Solid line corresponds to the most unstable mode and the dashed line corresponds to the second most unstable mode.

pressure eigenfunction and the symbols correspond to the case of homogeneous Neumann pressure boundary condition. Insensitivity of the results to the exact nature of the boundary condition is apparent, indicating that $\eta_{max} = \zeta_{max} = 25$ is adequately away from the corner region. Also plotted in this figure is the growth rate of the second most unstable model, whose maximum growth rate is nearly two and a half times smaller than that of the most unstable mode. The corresponding frequency variations are shown in figure 7 as a function of the streamwise wavenumber. A nearly linear increase in frequency with wavenumber can be observed. The frequency corresponding to the second most unstable mode is slightly smaller than that of the most unstable mode.

The inviscid instability mode with the largest growth rate corresponds to a streamwise wavenumber of $\alpha = 0.225$. This result compares well with results obtained from the bisector instability analysis, where α corresponding to the most amplified disturbance is 0.21 at $Re = 5000$ and very slowly increases with Reynolds number. The maximum growth rate (imaginary part of ω) obtained from the two-dimensional inviscid instability analysis is 0.004 and is much smaller than those obtained from the one-dimensional bisector instability analysis. This is because the mean flow in the two-dimensional analysis progressively becomes less inflectional away from the corner bisector and the overall effect is to reduce the growth rate in comparison with the one-dimensional analysis. The frequency (real part of ω) obtained from these two instability analysis agrees very well. For example, the non-dimensional frequency of the most amplified two-dimensional inviscid mode is 0.1 which compares well with $\omega_r = 0.089$ and 0.092 for the most amplified bisector modes at $Re = 5000$ and 4.5×10^4, respectively.

Figures 8(*a*) and 8(*b*) show the real and imaginary parts of the most amplified pressure eigenfunction ($\alpha = 0.225; \omega = 0.108 + i0.003975$). Peak values of the real part of the pressure eigenfunction occurs along the corner bisector near $\eta = \zeta = 2.5$ where the mean streamwise velocity profile is inflectional. Although the peak values of the

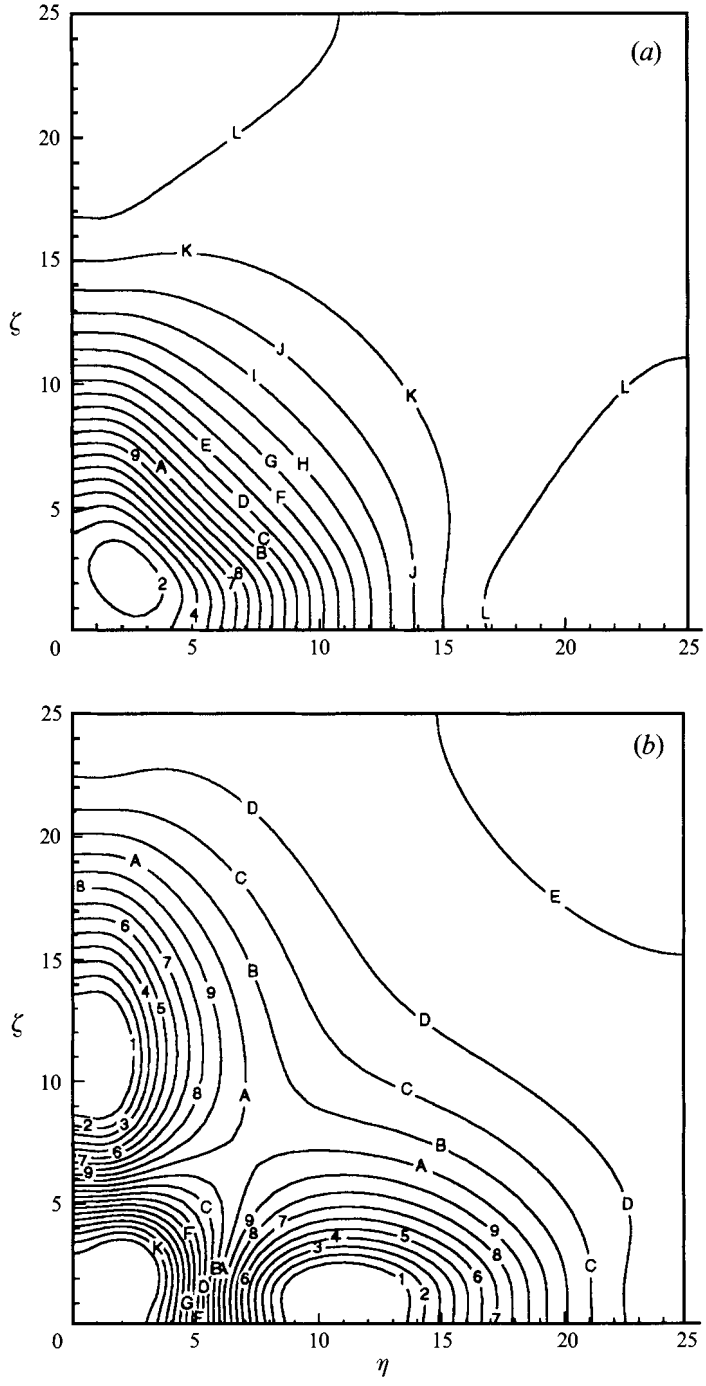

FIGURE 8. Contours of (*a*) the real and (*b*) the imaginary parts of the pressure eigenfunction corresponding to the most amplified inviscid disturbance. For the real part there are 21 contour lines ranging from −1.0 (marked 1) to 0 (marked L) and for the imaginary part there are 21 contours ranging from −0.2 (marked 1) to 0.1 (marked L).

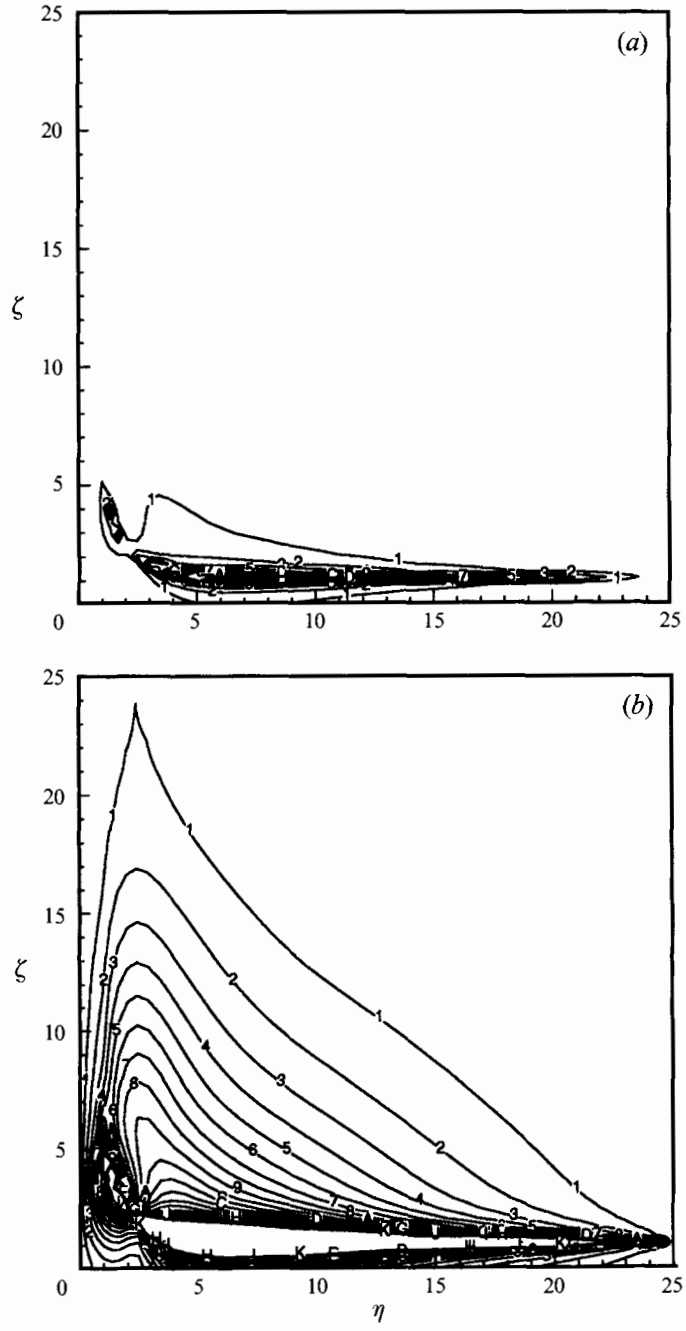

FIGURE 9. Contours of the absolute value of the v-velocity eigenfunction corresponding to the most amplified inviscid disturbance. For clarity the contours are plotted in two different ranges. In (*a*) there are 19 contours ranging from 1.0 (marked 1) to 19.0 (marked J) and in (*b*) there are 20 contours ranging from 0.1 (marked 1) to 2.0 (marked K).

imaginary part occur away from the corner bisector closer to the walls, the magnitude of the real part dominates the imaginary part. From the pressure eigenfunctions the corresponding velocity eigenfunctions can be evaluated based on (11). Figures 9(*a*) and 9(*b*) show contours of the v-eigenfunction plotted in two different ranges. It is clear

from this figure that the v-velocity of the disturbance rapidly increases near the critical layer where the denominator $i(\alpha\hat{u}_m - \omega)$ that occurs in the evaluation of the velocity eigenfunctions becomes nearly zero. But the pressure eigenfunction is well behaved in this critical layer region and therefore the eigenvalue computations are well resolved. The corresponding w-eigenfunctions can be obtained from figure 9 based on the even parity of the w- and v-eigenfunctions about the corner bisector.

4. Conclusions

Finally we conclude with a few comments on how the above results are relevant in explaining the rapid transition observed in zero-pressure-gradient corner flow experiments. The two-dimensional inviscid instability analysis, although confirming the possibility of an inviscid instability due to the inflectional nature of the mean streamwise velocity, does not provide any clue as to the critical Reynolds number for this mechanism to be active. On the other hand, the bisector instability analysis, although it ignores all variations in the mean flow away from the bisector, yields a critical Reynolds number of 435. In any case, these results suggest a possible destabilizing inviscid mechanism active starting from a point close to the leading edge as compared to the corresponding viscous instability in the Blasius boundary layer. These results are consistent with the experimental observations of Zamir (1981) that the corner flow becomes transitional at Reynolds numbers $\approx 10^4$ compared with the critical Reynolds number of $\approx 9 \times 10^4$ for the Blasius boundary layer.

This research was supported by the National Aeronautics and Space Administration under NASA Contract No. NAS1-19480 while the first author was in residence at the Institute for Computer Applications in Science and Engineering (ICASE), NASA Langley Research Center, Hampton, VA 23681-0001. Financial support for the second author was provided under NASA contract NAS1-19299. Work was completed during the Transition, Turbulence and Combustion Workshop co-sponsored by ICASE and NASA LaRC on June 7–July 2, 1993.

REFERENCES

BARCLAY, W. H. 1973 Experimental investigation of the laminar flow along a straight 135° corner. *Aeronaut. Q.* **24**, 147.

CANUTO, C., HUSSAINI, M. Y., QUARTERONI, A. & ZANG, T. A. 1988 *Spectral Methods in Fluid Dynamics*. Springer.

CARRIER, G. 1947 The boundary layer in a corner. *Q. Appl. Maths* **4**, 367.

DESAI, S. S. & MANGLER, K. W. 1974 Incompressible laminar boundary layer flow along a corner formed by two intersecting planes. *R.A.E. TR* 74062.

DHANAK, M. R. 1993 On the instability of flow in a streamwise corner. *Proc. R. Soc. Lond.* A **441**, 201.

EL-GAMAL, H. A. & BARCLAY, W. H. 1978 Experiments on the laminar flow in a rectangular streamwise corner. *Aeronaut. Q.* **29**, 75.

GHIA, K. N. 1975 Incompressible streamwise flow along an unbounded corner. *AIAA J.* **13**, 902.

GREGORY, N., STUART, J. T. & WALKER, W. S. 1955 On the stability of three-dimensional boundary layers with application to the flow due to a rotating disk. *Phil. Trans. R. Lond. Soc.* A **248**, 155.

HALL, P. & HORSEMAN, N. J. 1990 The inviscid secondary instability of fully nonlinear longitudinal vortex structures in growing boundary layers. *ICASE Rep.* 90-71.

LAKIN, W. D. & HUSSAINI, M. Y. 1984 Stability of the laminar boundary layer in a streamwise corner. *Proc. R. Soc. Lond.* A **393**, 101.

MACK, L. M. 1984 Boundary layer linear stability theory. *AGARD Rep* 709.

MALIK, M. R., WILKINSON, S. P. & ORSZAG, S. A. 1981 Instability and transition in rotating disk flow. *AIAA J.* **19** 1131.

PAL, A. & RUBIN, S. G. 1971 Asymptotic features of the viscous flow along a corner. *Q. Appl. Maths* **29**, 91.

PEARSON, J. R. A. 1957 Homogeneous turbulence and laminar viscous flow. PhD thesis, Cambridge University.

RUBIN, S. G. 1966 Incompressible flow along a corner. *J. Fluid Mech.* **26**, 97.

RUBIN, S. G. & GROSSMAN, B. 1971 Viscous flow along a corner: numerical solution of the corner layer equations. *Q. Appl. Maths.* **24**, 169.

STETSON, K. F., THOMPSON, E. R., DONALDSON, J. C. & SILER, L. G. 1983 Laminar boundary layer stability experiments on a cone at Mach 8. Part 1: Sharp cone. *AIAA Paper* 83-1761.

ZAMIR, M. 1981 Similarity and stability of the laminar boundary layer in a streamwise corner. *Proc. R. Soc. Lond.* A **377**, 269.

ZAMIR, M. & YOUNG, A. D. 1970 Experimental investigation of the boundary layer in a streamwise corner. *Aeronaut. Q.* **21**, 313.

ZAMIR, M. & YOUNG, A. D. 1979 Pressure gradient and leading edge effects on the corner boundary layer. *Aeronaut. Q.* **30**, 471.